Proceedings of the
44th IEEE Conference on Decision and Control, and
the European Control Conference 2005
Seville, Spain, December 12-15, 2005



# Control challenges in semiconductor nanostructure devices

Luis L. Bonilla and Ana Carpio

*Abstract*— **A superlattice is an artificial crystal made out by repeating periodically a basic unit comprising layers of two or more semiconductors. Superlattice based devices include infrared detectors, quantum cascade lasers and fast oscillators. A simple device consists of a finite superlattice with attached contacts and connected to an external circuit. If it is connected to a current source, the electric field profile inside the superlattice may be a wave front, which is possible to leave stationary or to move upstream or downstream of the electron flow depending on the value of the current. Under dc voltage bias, it is possible to attain stationary states or self-sustained oscillations of the current by controlling the voltage.**

## I. INTRODUCTION

There are many devices that are based on heterostructures grown by molecular beam epitaxy, i.e., by growing vertically layers of different semiconductor materials in a prescribed way. Among the simplest are the superlattices, which consist of a number of periods (having lengths in the nanometer range) each comprising two or more layers of different semiconductors [1]. Devices based on superlattices include high-frequency oscillators (up to several hundred GHz), detectors both in the THz and the infrared spectral regions, and infrared emitters (quantum cascade lasers) used to monitor atmospheric pollution by industries, to monitor bad breath in medicine applications, etc. For some of these devices, it is important to control their behavior which may be stationary or oscillatory depending on the value of the bias, the temperature, photoexcitation, etc [2], [3], [4], [5]. In this paper, we analyze the very simple example of a superlattice (SL) whose spatial period consists of only two layers (for example, GaAs and AlAs). The conduction band edge of an infinitely long ideal SL is modulated so that in the vertical direction it looks like a one-dimensional crystal, which is formed by a periodic succession of a quantum well (GaAs) and a barrier (AlAs). Typical experiments of vertical charge transport use an undoped or doped SL of finite length placed in the central part of a diode (forming a $p$-$i$-$n$ or $n^+$-$n$-$n^+$ structure) with respective contacts at either end of the diode. Depending on the bias condition, the SL configuration, the doping density, the temperature or other control parameters, the current through the SL and the electric field distribution inside the SL display a great variety of nonlinear phenomena such as pattern formation, current self-oscillations, and chaotic behavior, which can be exploited in different devices [5]. The simplest situation is that of a $n$-doped SL, in which electrons are the only carriers. Then the electronic spectrum consists of infinitely many minibands and gaps which can be calculated by solving the stationary Schrödinger equation for one electron with a periodic potential consisting of infinitely many square barriers and wells (the Kronig-Penney model). Charge transport in a device needs to include scattering between electrons and scattering of electrons with impurities, phonons, imperfections, etc. This is a complicated problem that should be treated within quantum kinetic theory. Posing and solving the corresponding equations are very difficult tasks, which is why a number of simplified models are used to understand different types of SLs. In this work, we shall consider SLs with wide barriers (called weakly coupled SLs because coupling between adjacent quantum wells is weak), in which the main mechanism of electron transport is sequential tunneling (see below). Charge transport can then be described by a system of differential-difference equations for the average electric field and the average electron density. These SLs still have interesting applications as oscillators, infrared detectors and emitters. In this paper, we consider the long time behavior of simple superlattice devices depending on current or voltage controls.

This work was supported by the MCyT grant BFM2002-04127-C02, and by the European Union under grant HPRN-CT-2002-00282.

L. L. Bonilla is with the Grupo de Modelización y Simulación Numérica, Escuela Politécnica Superior, Universidad Carlos III de Madrid, 28911 Leganés, Spain bonilla@ing.uc3m.es

A. Carpio is with the Departamento de Matemática Aplicada, Universidad Complutense de Madrid, 28040 Madrid, Spain ana_carpio@mat.ucm.es

## II. MODEL EQUATIONS

In weakly coupled SLs, the miniband widths $\Delta_\nu$ are small compared to the broadening of the energy levels due to scattering $\hbar/\tau_{sc}$, to the energy difference between minibands $(\mathcal{E}_\nu - \mathcal{E}_1)$ ($\mathcal{E}_\nu$ is the minimum energy of the miniband $\nu$), and to the typical values of the electrostatic energy per SL period $eFl$, in which $l$ is the length of one SL period, and $-e$ and $-F$ are electron charge and the electric field directed parallel to the growth direction, respectively. Then the electron distribution in the wells is in local equilibrium and the electrons occupy the lowest energy level of each well during most of the time [5]. Moreover, electrons move along the SL by tunneling across the barriers. For appropriate values of applied electric field $\tilde{F}_\nu = (\mathcal{E}_\nu - \mathcal{E}_1)/(el)$, $\nu = 1, 2, \ldots$, the electrons tunnel between the first level of one well and the level $\nu$ of the adjacent well, and then are scattered down to the first level of that well in a negligible time $\tau_{sc}$. This is called *resonant sequential tunneling* and yields peaks of the electron current across the SL for $F \approx \tilde{F}_\nu$. In the long time that the SL takes to react to a change in the electric field, $\tau_{sc}$ and the escape time $\hbar/\Delta_1$ can be ignored and the tunneling current can be considered to be a function of the local values of the field and the electron density. Then the following simple discrete model of transport is valid.

Consider a SL with $N+1$ barriers and $N$ wells. The zeroth barrier separates the injecting region from the first SL well, whereas the $N$th barrier separates the $N$th well from the collecting region. Assume that $F_i$ is the average field across one SL period (note that the actual electric field is $-F_i$), consisting of the $i$th well and the $(i-1)$th barrier. Similarly, $n_i$ is the 2D electron density at the $i$th well, concentrated in a plane perpendicular to the growth direction inside the $i$th well. Then, the Poisson equation (averaged over the $i$th period) and the charge continuity equation are

$$F_i - F_{i-1} = \frac{e}{\varepsilon}\,(n_i - N_D). \tag{1}$$

$$e\,\frac{dn_i}{dt} = J_{i-1\to i} - J_{i\to i+1}. \tag{2}$$

Here $J_{i\to i+1}$ is the tunnelling current density across the $i$th barrier, i.e. from well $i$ to well $i+1$ with $i = 1,\ldots,N$. The parameters $\varepsilon$ and $N_D$ are the SL average dielectric constant and doping density, respectively. Differentiating (1) with respect to time and inserting the result into (2), we obtain

$$\varepsilon\frac{dF_i}{dt} + J_{i\to i+1} = J(t), \tag{3}$$

in which the total current density $J(t)$ is the same function for all $i$. Equation (3) is a discrete version of Ampère's equation. We shall now assume that $J_{i\to i+1}$ depends on $F_i$, $n_i$, and $n_{i+1}$. The tunnelling current across the $i$th barrier clearly depends on the electrochemical potentials of the adjacent wells, thereby depending on $n_i$ and $n_{i+1}$. That $J_{i\to i+1}$ depends on $F_i$, but not on $F_{i+1}$, is a simplifying assumption. We complete our description by adding the *voltage bias* condition

$$\frac{1}{(N+1)}\sum_{i=0}^{N} F_i \;=\; \frac{V(t)}{(N+1)l}\,, \tag{4}$$

for the known voltage $V(t)$. Another possible bias condition consists of fixing the total current density $J(t)$, which is called *current bias*.

Our discrete system of equations consists of (1) for $i = 1,\ldots,N$, (3) for $i = 0,\ldots,N$, and (4). In total, we have $(2N+2)$ equations for the unknowns $n_1$, …, $n_N$, $F_0$, …, $F_N$, and $J(t)$. We need to derive the constitutive relations $J_{0\to 1}$ (tunnelling from the injecting region to the SL), $J_{i\to i+1}$ (tunnelling across an inner barrier of the SL), and $J_{N\to N+1}$ (tunnelling from the SL to the collecting region). Equation (3) evaluated for $i = 0$ and $i = N$ determines the boundary conditions.

The functions $J_{i\to i+1} = \mathcal{J}(F_i, n_i, n_{i+1})$ can be calculated by using different approximations of quantum kinetic theory. Convenient explicit expressions are given in Appendix A of [2]. It is important to note that $\mathcal{J}(F_i, N_D, N_D)$ has local maxima at $F \approx \tilde{F}_\nu$, $\nu = 2,\ldots$. The tunneling current has its lowest maximum at a positive field $F = F_M < \tilde{F}_2$. In the high-temperature limit $k_BT \gg \pi\hbar^2 n_{i+1}/m^* \approx \pi\hbar^2 N_D/m^*$ ($k_BT$ and $m^*$ are the thermal energy and the effective mass of the electron, respectively), the tunneling current density can be approximated by the discrete drift-diffusion form [2]

$$J_{i\to i+1} = \frac{e\,n_i\,v(F_i)}{l} - \frac{e\,D(F_i)}{l^2}\,(n_{i+1} - n_i) \tag{5}$$

$$v(F_i) = v^{(f)}(F_i)\,\left(1 - e^{-\frac{eF_il}{k_BT}}\right) \tag{6}$$

$$D(F_i) = v^{(f)}(F_i) l e^{-\frac{eF_il}{k_BT}}\,, \tag{7}$$

in which $v^{(f)}(F_i)$ is a sum of Lorentzians centered at the resonant field values $\tilde{F}_\nu = (\mathcal{E}_\nu - \mathcal{E}_1)/(el)$.

Appropriate simplified boundary conditions $J_{0\to 1}$ and $J_{N\to N+1}$ are

$$J_{0\to 1} = \sigma F_0, \quad J_{N\to N+1} = \sigma F_N \frac{n_N}{N_D}\,, \tag{8}$$

in which the positive parameter $\sigma$ is the contact conductivity, selected so that the straight line $J = \sigma F$ intersects $\mathcal{J}(F, N_D, N_D)$ on its second decreasing branch at a point $(F_c, J_c)$ with $F_M < F_c < F_m$. $F_m$, $F_M < F_m < \tilde{F}_2$, is the field at which $\mathcal{J}(F, N_D, N_D)$ reaches its local minimum.

## III. LONG TIME BEHAVIOR AT CONSTANT CURRENT BIAS

If the current across the SL is constant, $J(t) = J$, an initial field profile evolves towards a time-independent configuration. For sufficiently large $N$, the influence of the boundary conditions is limited to a few periods near the contacts. Ignoring these regions, stable stationary field profiles are either constant functions $F_i = F^{(n)}$ solving

$$\mathcal{J}(F, N_D, N_D) = J, \tag{9}$$

or monotone field profiles joining two solutions of (9). This can be easily proved by linear stability arguments or using the comparison principle [6]. If we consider positive current values $0 < J < J_M = \mathcal{J}(F_M, N_D, N_D)$, and restrict field values to the interval $0 < F < \tilde{F}_2$, the possible stable field configurations are as follows.

- For $0 < J < J_m = \mathcal{J}(F_m, N_D, N_D)$, $F = F^{(1)}(J)$, which is the only solution of (9).
- For $J_m < J < J_M$, there are three solutions $F^{(1)}(J) < F^{(2)}(J) < F^{(3)}(J)$ of (9), and $F_i = F^{(1)}(J)$ and $F_i = F^{(3)}(J)$ are linearly stable profiles. Other linearly stable profiles $F_i$ are monotone functions of $i$ joining regions where $F_i \approx F^{(n)}(J)$, $n = 1, 3$. These regions of approximately constant field value are called *electric field domains* (EFD). The transition regions of intermediate field values between two EFDs are called domain walls. Wave fronts are moving domain walls.

Typically, initial field profiles with several EFDs evolve towards either a constant field profile or towards a stationary profile having one domain wall and two EFDs. During the transient period, domain walls move towards the boundaries or annihilate each other. To further analyze the motion of domain walls, it is convenient to consider the case of an infinitely long SL.

*1) Pinning in current-biased, infinite SLs:* Let us consider the theory of wave fronts in current-biased, infinite SLs. The main difference between wave fronts of spatially discrete and continuous autonomous equations (no imperfections or spurious time- or space-dependent coefficients) is the phenomenon of pinning. Roughly speaking, wave fronts of continuous equations have to move (except at single values of a control parameter that characterizes their non-linearities), whereas wave fronts of discrete equations can be pinned for entire intervals of their control parameter. In the case of the SLs, the current is the control parameter [6].

The pinning and the motion of wave fronts (domain walls) are illustrated in figures 1 and 2. The results shown in these figures have been obtained from stable solutions of the discrete model with drift-diffusion tunnelling currents as in (5). Figure 1 depicts the velocity of a wave front moving at constant speed in a doped, infinite SL under constant current-bias conditions. For the doping density of this SL, wave fronts having a spatially decreasing profile of the electric field move from left to right, i.e. *downstream*, with velocity $c^-$, following the motion of individual electrons for any value of the current. These wave fronts correspond to moving charge depletion layers (CDLs). The behavior of wave fronts having an increasing field profile, and thus corresponding to charge accumulation layers (CALs), is more interesting. Below a first critical current $J_{c1}$, the wave front moves downstream too, and their velocity is $c^+$. There is an interval of currents, between the first and the second critical currents, in which the wave front has zero velocity: it is pinned in a well, whose position depends on the initial conditions of the numerical simulation. For currents larger than the second critical current, the wave front moves *upstream*, against the motion of single electrons [6]. Near the critical currents, the evolution of the electric field in a single or in several wells determines the pinning/depinning transition according to the active well theory described in [7], [2]. As the current approaches one of its critical values from the side corresponding to moving fronts, the electric field profile acquires a step-like appearance. The steps become infinitely long, and the wave front is pinned at the critical currents [7]. The wave front velocity approaches zero as the square root of $|J - J_c|$.

Figure 2 shows that the existence of wave front pinning depends on the SL doping density. Below a first critical doping density, all CALs move downstream (just as in continuous models of strongly coupled SLs or in the Gunn effect). A useful lower bound for the first critical doping density is [6]

$$N_D > \frac{\varepsilon\,(F_m - F_M)}{e}\,\frac{v_m}{v_M - v_m}, \tag{10}$$

where $v_M = J_M l/(eN_D)$ and $v_m = J_m l/(eN_D)$ are the local first maximum and minimum of the drift velocity $v(F)$. To obtain a lower bound of the doping density, above which pinning of CDLs is possible, we have to substitute $v_M$ instead of $v_m$ in the numerator of (10) [8]. Between the first and a second critical doping density, CALs can be pinned or move downstream depending on the current. Lastly, above the second critical doping density, the wave fronts may also move upstream [6]. Note that the pinning interval increases with an increasing SL doping density.

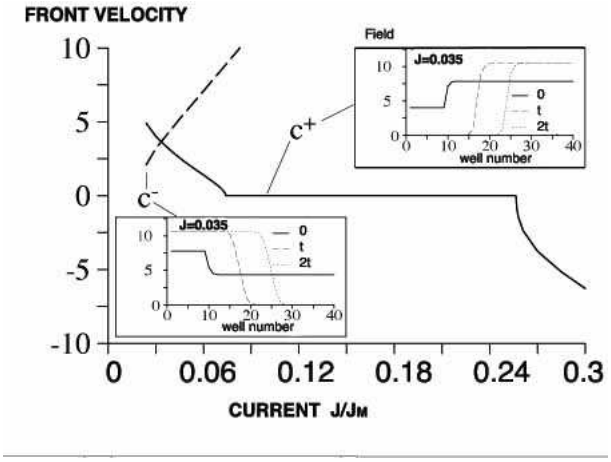


Fig. 1. Velocities of wave fronts shown in the inset versus current bias $J$ (in units of $J_M$). The parameters of the GaA/AlAs SL are well width: 9 nm, barrier width: 4 nm, $l = 13$ nm, $N_D = 1.5{\times}10^{15}$ m$^{-2}$, and $S = 1.13{\times}10^{-8}$ m$^2$. Then $F_M = 7.69{\times}10^6$ V/m, and $J_M = 2.88{\times}10^4$ A/m$^2$. Adapted from [3].

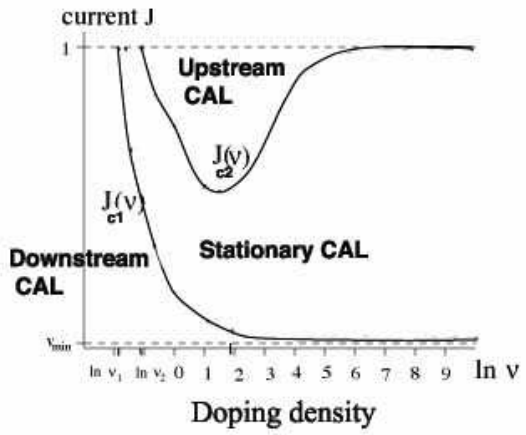


Fig. 2. Critical currents $J_{c1}$ and $J_{c2}$ (in units of $J_M$) versus logarithm of the dimensionless doping density $\nu = eN_D/(\varepsilon F_M)$. Adapted from [6].

*2) Controlling wave front motion:* The analysis of the phase diagram in Fig. 2 [6] yields the following Theorem:

*There exist two critical values of the doping density, $0 < \nu_1 < \nu_2$, and two critical currents, $0 < J_{c1}(\nu) < J_{c2}(\nu)$ ($J_{c1}$ is defined for $\nu > \nu_1$ and $J_{c2}$ is defined for $\nu > \nu_2$), such that:*

- *Choosing $\nu < \nu_1$, or $\nu > \nu_1$ and $J < J_{c1}(\nu)$, CAL domain walls propagate downstream following the flux of electrons.*
- *Choosing $\nu_1 < \nu < \nu_2$ and $J > J_{c1}(\nu)$, or $\nu > \nu_2$ and*

$J_{c1}(\nu) < J < J_{c2}(\nu)$, *CAL domain walls are pinned.*

- *Choosing* $\nu > \nu_2$ *and* $J > J_{c2}(\nu)$, *CAL domain walls move upstream, against the flux of electrons.*

The critical currents $J_{c1}(\nu)$ and $J_{c2}(\nu)$ are characterized by a bifurcation analysis, which also yields an approximate formula for the velocity of the wave fronts for currents close to the critical values [7].

## IV. LONG TIME BEHAVIOR AT CONSTANT VOLTAGE BIAS

At constant voltage bias, the stable field configurations are either stationary or oscillatory, typically time-periodic. The time-periodic current density and field profiles can be interpreted in terms of periodic motion of wave fronts, as described in [5]. Except close to contacts, stationary field profiles are either constant or monotone profiles having two EFDs separated by a domain wall. They are the same profiles as for current bias, but now the current is a function of voltage $V(t) = V$ obtained by entering the considered field profile as function of $J$ in the bias condition (4), and then solving this equation for $J$ with fixed $V$. A typical outcome of these calculations for appropriate parameter values (for example, for appropriate values of the doping density) is that there are several branches of stationary solutions for each value of $V$. Two or more of these stationary solutions are stable, and the final field profile depends on the initial condition.

To determine the effect that the configuration and SL doping density have on the static and oscillatory solutions of a discrete model, it is convenient to draw a doping density-voltage phase diagram as in figure 3. This is a diagram for the second plateau, i.e. zero diffusivity, of a 20-period SL, assuming that $D(F_i) = 0$ and a boundary condition $n_1/N_D = 1 + c$ with $c = 10^{-4}$ [9]. Static and oscillatory behaviors of the SL for this boundary condition are similar to those obtained using (8) for sufficiently large values of $\sigma$ so that $J = \sigma F$ does not intersect the curve $J = ev(F)N_D/l$ [5]. For a dimensionless doping density $\nu = eN_D/(\varepsilon F_M)$ lower than the minimum of the solid line, the stable field profile is stationary and almost uniform ($F_i = F^{(1)}(J)$ except very close to $i = 0$). For larger doping densities, with $\nu < \nu_{TB}$, the almost uniform stationary state is linearly stable outside a certain bias interval of average dimensionless field values $\phi_\alpha < \phi < \phi_\omega$, with $\phi = V/[(N+1)F_M l]$. At the end points of this voltage interval, a branch of self-oscillations stably bifurcates (supercritically) starting with zero amplitude and non-zero frequency (Hopf bifurcation). For $\nu > \nu_{TB}$, a horizontal line of constant doping density intersects a number of different curves: (i) Hopf bifurcations (dashed line: subcritical Hopf bifurcation, solid lines: supercritical Hopf bifurcations), (ii) saddle-node bifurcations, and (iii) homoclines. At the Takens-Bogdanov point TB, lines of Hopf bifurcations, saddle-node bifurcations and homoclinic orbits intersect tangentially.

The intersection of the horizontal line with several Hopf bifurcation curves may indicate that there are intervals of self-oscillations alternating with intervals, in which the stable

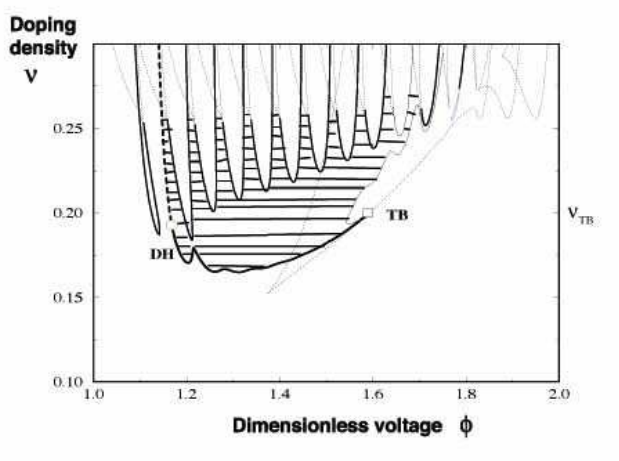


Fig. 3. Total phase diagram of the discrete model for $N = 20$. The dotted lines are curves of stationary saddle nodes. For the sake of clarity, we have plotted only the main line of homoclinic orbits (thin solid line), which originates from the Takens-Bogdanov point TB. We have not shown other homoclinic orbits, although there is one curve of homoclinic orbits for each Hopf curve. Adapted from [9].

solution is a stationary state with two EFDs separated by a domain wall. There may be at most $N$ intervals of stable stationary states, and the CAL separating the LFD and the HFD is pinned at a different well $i$ in each different voltage interval. Let us consider the bias interval of self-oscillations located between intervals, whose corresponding static CALs are pinned at wells $i$ and $(i+1)$. The field profile for these oscillatory states corresponds to a recycling and motion of a CAL about the $i$th well. In some of the interior regions observed for such doping densities, there may be coexisting multistable states.

The interval of self-oscillations with largest bias ends at a homocline, i.e. the oscillation frequency tends to zero, while the amplitude remains finite. Another interesting feature of the phase diagram is the dashed line of Hopf bifurcations above the point marked DH. On this line, the Hopf bifurcation is subcritical, i.e. an unstable branch of self-oscillations bifurcates for $\phi < \phi_\alpha$. Typically this branch coalesces with a branch of stable oscillations at a smaller bias $\phi_{LP}$. Then there is a bias interval of bistability, in which both self-oscillations of finite amplitude and frequency as well as a stationary state are stable. Driving adiabatically the bias, we can obtain a hysteresis cycle. Finally, for a sufficiently large doping density, the self-oscillations disappear, and the result is multistability of stationary solutions corresponding to coexistence of EFDs separated by a pinned CAL.

The phase diagram in figure 3 may substantially change, if we change the number of SL periods or the boundary condition (e.g, the parameter $c$). For example, the branch of self-oscillations may disappear at the high bias region either at a Hopf bifurcation (finite frequency) or at a homoclinic orbit (zero frequency), depending on the values of these parameters.

*3) Controlling oscillations:* The analysis of the phase diagram in Fig. 3 [9] yields the following Theorem:

*There is a connected region in the phase plane of the control parameters $\phi$ (dimensionless average field) and $\nu$ (dimensionless doping density) such that selecting $(\nu, \phi)$ in this region, the stable solution of the model equations is time-periodic (corresponding to self-sustained oscillations of the current through the superlattice). If the control parameters are selected outside the same region, the stable solutions are stationary.*

The region corresponding to self-sustained oscillations is shaded in Fig. 3. Its upper and lower boundaries are Hopf bifurcation lines, whereas its right-most boundary is the line of homoclines. If the number of SL periods or the boundary condition are changed, the details of the shaded region may change. Note that if we fix the doping density near the upper boundary of the oscillation region, intervals of oscillatory and stationary behavior alternate as $\phi$ increases. Similar behaviors occur if temperature or photoexcitation are used as control parameters instead of the doping density [5].

## V. CONCLUSIONS AND CHALLENGES

Long time behavior of a weakly coupled, doped superlattice depends on boundary conditions and control parameters, notably in the bias conditions. Under constant current bias, stable solutions have field profiles comprising two electric field domains separated by a domain wall. By changing the current, the motion of the domain wall can be directed towards either end of the superlattice or the domain wall can be pinned. Under constant voltage bias, the long time behavior of the superlattice is either stationary or time-periodic, corresponding to a pinned domain wall or to periodically moving domain walls. By changing doping density and the voltage, either behavior can be selected.

There are other control parameters that have been kept fixed, and therefore their influence on the SL behavior has been ignored. Among them, let us quote the lattice temperature, the photoexcitation, the contact conductivity and an applied magnetic field. Most of the work concerning the influence of these parameters on the SL behavior has been carried out by experimentalists, and our theoretical understanding lags behind experimental results [5]. Phase diagrams similar to that in Fig. 3 should be calculated and interpreted along similar lines.

Strongly coupled SLs provide examples of faster oscillations than weakly coupled SLs. However, better kinetic models than those known today should have to be proposed and worked out before a similarly detailed theory for controlling these oscillators is developed [5]. In particular, much more modeling work on high field electronic transport involving several minibands of the SL is needed.

## VI. ACKNOWLEDGMENTS

We thank Michele Pavon for inviting us to the minisymposium on Control of Physical Systems within ECC 2005, and encouraging us to present our results.

## REFERENCES

[1] H. T. Grahn (ed.), *Semiconductor Superlattices: Growth and Electronic Properties*, World Scientific, Singapore; 1995.

[2] L. L. Bonilla, Theory of nonlinear charge transport, wave propagation, and self-oscillations in semiconductor superlattices, *J. Phys.: Condens. Matter*, vol. 14, 2002, pp R341-R381.

[3] A. Wacker, Semiconductor superlattices: A model system for nonlinear transport, *Phys. Rep.*, vol. 357, 2002, pp 1-111.

[4] G. Platero and R. Aguado, Photon-assisted transport in semiconductor nanostructures, *Phys. Rep.*, vol. 395, 2004, pp 1-157.

[5] L. L. Bonilla and H. T. Grahn, Nonlinear dynamics of semiconductor superlattices, *Rep. Prog. Phys.*, vol. 68, 2005, pp 577-683.

[6] A. Carpio, L. L. Bonilla, A. Wacker and E. Schöll, Wavefronts may move upstream in semiconductor superlattices, *Phys. Rev. E*, vol. 61, 2000, pp 4866-4876.

[7] A. Carpio, L. L. Bonilla and G. Dell'Acqua, Motion of wave fronts in semiconductor superlattices, *Phys. Rev. E*, vol. 64, 2001, 036204-1–036204-9.

[8] A. Wacker, M. Moscoso, M. Kindelan and L. L. Bonilla, Current-voltage characteristic and stability in resonant-tunneling n-doped semiconductor superlattices, *Phys. Rev. B*, vol. 55, 1997, pp 2466-2475.

[9] M. A. Moscoso, J. Galán and L. L. Bonilla, Bifurcation behavior of a superlattice model, *SIAM J. Appl. Math.*, vol. 60, 2000, 2029-2057.